WIS-94/11/Feb.-PH
SW 9416

Field enhancement of the photoelectric and secondary electron emission from CsI

A.Buzulutskov* , A.Breskin and R.Chechik
Department of Particle Physics
The Weizmann Institute of Science, 76100 Rehovot, Israel

Abstract

We have measured the electron emission from a CsI-coated multiwire cathode, induced by UV-photons and electrons, in vacuum at high electric fields. We found an enhancement in quantum efficiency of a factor of 1.5 at 160 nm, 3 at 185 nm and 25 above 200 nm, at a field of 500 kV/cm. At the short wavelengths the amplitude of the effect is a linear function of the square root of the field strength. The enhancement of the electron-induced secondary electron emission yield is dependent on the primary electron energy: for energies above 1 keV it varies by a factor of 2 to 10. A simple model of the field enhancement of the photoemission is suggested. Practical applications are discussed.

Submitted to the Journal of Applied Physics

*on leave of absence from IHEP, Protvino, Russia

1 Introduction

The growing interest in CsI as an electron emission material is due to its high quantum efficiency (QE) in the UV range [1, 2, 3, 4], a high secondary electron emission (SEE) yield [5, 6], a relatively high stability in air [7] and its capability to operate in a stable way in combination with gaseous imaging electron multipliers [8, 9].

These properties make CsI a promising photoconvertor for UV-photon or X-ray imaging [10, 11]. Though the electron emission from CsI has been actively investigated during last years, there are still some open questions concerning its dependence on various experimental factors (see discussion in [3]). In our recent work [12] we have studied for example the influence of the electric field on the QE, in gas media, at relatively low field values (below 10 kV/cm).

In the present work we investigate the CsI emission properties at very high electric fields, reaching 500 kV/cm, in vacuum. The field enhancement of the electron emission was systematically studied in the past for semiconductor photocathodes used in proximity-focused image tubes, at electric fields up to 70 kV/cm [13, 14], and for porous alkali halide films used as secondary electron emitters, at electric fields up to 30 kV/cm [15, 16].

The present study has been initiated following some observations that after a gas breakdown [12] or under a high photon flux [17, 18, 19] the QE value of CsI considerably increases. This enhancement could have resulted from positive ion deposition on the CsI surface following discharges due to a large local avalanche: since CsI is generally an insulator, the positive ions can not be rapidly neutralized and therefore they are accumulated in nonconductive regions of CsI. This can result in the creation of rather high local electric fields, of the order of several hundreds of kV per cm. We supposed [12] that this field is responsible for an enhancement of the photoelectron extraction probability due to a decrease of the electron work function, simalar to the Schottky effect in metals.

The first goal of the present work was to check this hypothesis. The other goal was to try to understand, in a more general aspect, the effect of the electric field on the electron emission from CsI, induced by photons or energetic electrons. This understanding could help one to predict the electron emission properties of other insulators under high electric fields. We present a model which describes the field-enhanced photoemission process. We also discuss here some practical applications of the field enhancement effect.

2 Experimental setup

To obtain very high electric fields, reaching several hundreds of kV/cm in vacuum, we used a multiwire plane cathode, placed between two mesh anode planes. Electric fields in such a structure, which is very simalar to that used in multiwire proportional chambers [20], are well defined and can be calculated analitically [21]. Using a CsI-coated multiwire

cathode, two basic sets of measurements were carried out: UV-induced photoelectric emission (photoemission) and electron-induced secondary electron emission (SEE).

The wire-photocathode was prepared by an evaporation of a CsI layer on one side of the wire grid in vacuum of 10^{-6} Torr. The CsI layer on the wire has a crescent moon shape with a maximum thickness at the center of 500 nm. The grid had an active area of 80 mm in diameter and was made from Au-plated tungsten wires of 10 μm diameter with a 1 mm spacing. After evaporation, the photocathode was transported to the chamber, the exposure time to air being about 10 min. Two wire-photocathode samples were prepared: one was used for both experiments, while the other was used only for the photoemission experiment.

2.1 The photoemission setup

A schematic view of the setup for the photoemission experiment is shown in Fig.1a. Two UV sources were used: a Hg(Ar) lamp and a D_2 lamp. UV-photons from the Hg(Ar) lamp, placed in air, enter the vacuum chamber through a quartz window. The D_2 lamp had a MgF_2 window and was placed within the chamber. The emission spectra of the lamps have been measured with the help of a monochromator. The most pronounced emission lines of the Hg(Ar) lamp are at 185 nm and 254 nm; no other significant lines were detected between these two peaks. The emission spectrum of the D_2 lamp has an intense peak at 160 nm, with a FWHM of about 10 nm, and a rather flat continuum extending to wavelengths above 250 nm.

The wire-photocathode was placed between two stainless steel meshes, 81% transparent, at a distance of 3.2 mm. The meshes were under a positive voltage, while the photocathode was grounded through a picoampermeter.

The diameter of the light spot at the photocathode plane was of the order of 20-50 mm. A photon flux density at the wire plane was estimated to be of the order of 10^8 photons/sec·mm^2 at 185 nm while using the Hg(Ar) lamp, and about 10^9 photons/sec·mm^2 at 160 nm while using the D_2 lamp. Note, that only 1% of the photons hit the photocathode wires.

The measurements were made in vacuum of $3 \cdot 10^{-5}$ Torr.

2.2 The secondary electron emission setup

The secondary electron emission experiment was carried out in the same setup, but with two modifications (see Fig.1b). First, a plate CsI photocathode was installed at a distance of 7 mm from the anode mesh; it acted as a primary electron source, as described below. Second, the cathode wire plane was turned around, so that the CsI layer faced the plate CsI electrode; it acted as a SEE-cathode. During this procedure both CsI cathodes were once more exposed to air for about 10 min.

The plate CsI photocathode was kept under negative voltage $-U_{pc}$. Primary electrons emmited from the plate under UV-radiation, were first accelerated in a photocathode/anode gap and then decelerated in the anode/wire-cathode gap. The resulting primary electron energy E_p, inducing secondary electron emission at the cathode wires, was equal to $E_p = eU_{pc}$. Thus the voltage on the photocathode determined the energy of the primary electrons, while the voltage on the anodes determined the electric filed strength F at the SEE-cathode wires surface. A primary electron flux density at the SEE-cathode was estimated to be of the order of $5 \cdot 10^6$ electrons/sec·mm^2.

3 Experimental results

3.1 Photoemission

The UV-induced photocurrent from CsI was measured as a function of the mesh voltage U_a; it typically amounted to several hundreds of picoamperes for a fresh photocathode. The dark current was substracted from each measured value. It typically amounted to several picoampers and was independent of the voltage. Due to a high stability of the incident photon flux, the photocurrent can be considered to be proportional to the quantum efficiency (QE) of the photocathode investigated.

The field strength value on the wire surface was calculated according to the expression [21]:

$$F = \frac{U_a}{\pi l/s - ln(\pi d/s)} \cdot \frac{1}{d/2} \qquad (1)$$

where U_a is the anode voltage, l the anode-to-cathode distance, s the cathode wire spacing, d the cathode wire diameter.

Fig.2 shows a relative quantum efficiency of the wire-photocathode as a function of the electric field strength, measured with a Hg(Ar)lamp. The first data set presented in the figure, was measured with a fresh CsI wire-photocathode. All data points are normalized to the point at the lowest field value, measured for this photocathode. One can see a dramatic dependence of the QE on the field: at the field of 400 kV/cm the QE value increases by a factor of 2.5 compared to that at the low field region.

To study the relative contribution of the 254 nm line to the photocurrents, we have suppressed this line using a wavelength filter. No difference in the QE dependence on the field was observed in this case, meaning that the photocurrent is induced by 185 nm photons only.

The second data set shown in Fig.2, was obtained after several investigations including the secondary electron emission experiment described below. The wire-photocathode could have been aged by electron bombardment. The QE values of the aged photocathode was measured to be 5 times lower than those of the fresh photocathode. Nevertheless, as

one can see from Fig.2, the general behaviour of the aged photocathode did not change: at the field of 500 kV/cm the QE enhancement is of the order of 3.

To check that the field enhancement is not due to secondary processes in the residual gas like charge multiplication, several measurements were made at different vacuum levels, ranging from 10^{-5} to 10^{-3} Torr. No dependence of the effect on the vacuum level was found. We also did not observe any dependence of the effect on the photon flux when reducing the flux by an order of magnitude.

The field enhancement effect at different wavelengthes was studied with another wire-photocathode. No significant difference was observed between this and the previous photocathode samples at 185 nm, when using the Hg(Ar)lamp. When using the D_2 lamp, wavelength cut-off filters were used to select either the 160 nm emission peak or the wavelength region above 200 nm. The results of these measurements are shown in Fig.3.

It is interesting to note that the QE enhancement at 185 nm and 160 nm is a linear function of the square root of the electric field strength over a wide field range (Fig.3a). This is not the case for the wavelengths near the QE red boundary of CsI and for longer wavelengthes (Fig.3b): the QE increases with field much faster. The amplitude of the QE enhancement increases with the wavelength, varying, at the field of 500 kV/cm, from a factor of 1.5 at 160 nm, to 3 at 185 nm and to about 25 above 200 nm. A possible explanation to these dependences is presented in section 4.

The QE enhancement for the wire-photocathode measured at low fields, up to 10 kV/cm, is about 10-20% at 185 nm. This is in coherence with our and others [22] observations in a parallel-plate geometry. It confirms that even at low fields a voltage plateau of the QE in vacuum is not fully flat.

3.2 Secondary electron emission

3.2.1 Background and aging

A secondary electron emission current from the CsI wire cathode (SEE-cathode) was measured as follows. The current detected from this electrode, J_c, is a sum of the SEE-currents from CsI, $J_{SEE}(CsI)$, induced by primary electrons and the "background" current J_b:

$$J_c = J_{SEE}(CsI) + J_b \tag{2}$$

J_b is a combination of several currents:

$$J_b = J_p + J_{UV} + J_m \tag{3}$$

J_p results from primary electrons hitting the cathode wires; J_{UV} is a photocurrent induced by UV-photons reflected from the anode mesh and from the CsI plate; J_m is a current resulting from electrons induced by primaries hitting the mesh anodes.

The contributions of J_{UV} was found negligible; it was measured by applying a retarding positive potential to the plate-photocathode, thus eliminating the primary electrons. It turned out that at some voltages J_b was comparable to J_c, the main contribution being from J_m: though the SEE-yield of metal (of which the anode meshes are made) is low compared to that of CsI, the total active anode area is about two orders of magnitude larger than that of the CsI SEE-cathode. Thus, there exists an appreciable probability for electrons, emitted or reflected from the anode meshes, to reach the cathode wires and to initiate a secondary emission background from CsI.

The contributions of J_p and J_m were measured in the following way. The SEE-cathode plane was turned around, back to the position used in the photoemission experiment, so that the primary electrons hit the metal side of the wires, not covered with CsI. Due to the symmetry of the geometry used, the measured current in that position is

$$J'_c = J_{SEE}(Me) + J_p + J_m + J'_{UV} \tag{4}$$

where J'_{UV} was measured in a simalar way as before; $J_{SEE}(Me)$ is the SEE-current from the metal side of the cathode wires (presumably from gold) induced by the primary electrons (see Fig.1b).

Using the expressions (2)-(4), we determined, for each voltage applied to the anodes and the plate-photocathode, the current

$$J_{SEE} = J_c - J'_c + J'_{UV} - J_{UV} = J_{SEE}(CsI) - J_{SEE}(Me) \tag{5}$$

We define this current, resulting from the difference between the CsI and metal SEE-currents, as the "SEE-current". This SEE-current is proportional to the SEE-yield, defined as the number of the secondary electrons emitted per primary electron, if the primary electron flux does not change during the measurements. Since the ratio of total SEE-yields from metals and CsI is typically below 10% [5], one may approximate the $J_{SEE}(CsI)$ by the J_{SEE}.

To take into account a possible reduction of the primary electron flux due to the CsI plate-photocathode degradation under high UV-photon flux, all measured parameters were corrected, taking into account the current recordered in the photocathode circuit. The primary electron flux can also be dependent on the voltage, due to a repulsive potential on the wires. Our estimations showed that in the range of electric fields studied, repulsive forces near the wire are important only for electrons with the energies below 20 eV.

Since the values of the primary electron flux and that of the SEE-current were rather high, one should take into account aging effects of the SEE-cathode. No significant decrease of the SEE-yield was observed. We also did not observe any fast decrease in QE, when irradiating with UV-photons. However, under a bombardment by a few keV electrons, the QE at 185 nm dropped rather fast down to 25% of its initial value. As was mentioned above, this drop did not affect the relative value of the field enhancement of the QE.

3.2.2 SEE-yield dependence on the field and on the primary electron energy

Fig.4 shows the relative SEE-yield from CsI, measured as described in the previous section, as a function of the primary electron energy, at three different field values at the wire SEE-cathode: 1.5, 15 and 150 kV/cm. For comparison, typical data of the total SEE-yield of CsI, measured at low fields with a plate SEE-cathode, are presented as well [23].

The behaviour of the energy dependence of our data, at low field, is in agreement with that of ref. [23], for primary electrons with energies below 3 keV. However, for higher energies, the SEE-yield in our measurements decreases with energy more rapidly, reaching a constant value. This difference may result from the different geometries used. Indeed, the plate SEE-cathode, used in typical SEE experiments, undergoes a normal incident flux. It is rather thick and has practically an infinite size in the direction orthogonal to the beam. This is not the case for the wire SEE-cathode: the incident angle varies from zero to 90 degrees and the size of medium is limited in the lateral direction, being dependent on the incident point. Geometrical effects are particularly important at higher energies, where a secondary electron cascade can be too large to be confined within the CsI layer. For example, according to ref. [24], 5 keV electrons induce in an infinite CsI volume a cascade having drop-like shape of about 500 nm in diameter. Obviosly, such cascade cannot be confined within the crescent moon-shaped layer coating our wire, having a maximum thickness of 500 nm.

Fig. 5 shows the relative SEE-yield for three different primary electron energies, as a function of the electric field strength at the wire surface. The data presented in Fig.4 and 5 were obtained in different measurement sets, which allows us to estimate the systematic errors. The averaged systematic error is shown for some data points.

Looking at Fig.4 and 5, we can draw some general conclusions:

- For low electron energies, of the order of 100 eV, the SEE-yield is independent of the field.
- In the energy range of 1-3 keV the SEE-yield rapidly increases by a factor of 2, when increasing the field from 1 to 10 kV/cm. At 1 keV the SEE-yield tends to saturate with a further field increase.
- For electron energies higher than 5 keV the SEE-yield dramatically increases by an order of magnitude, when increasing the field from 1 to 10 kV/cm. It further increases with the field following a logarithmic law.

4 Discussion

4.1 A simple model for the field enhancement of the photoelectric emission

The field enhancement of the photoemission in semiconductor photocathodes, mentioned in the introduction, was accounted for by a change of the work fuction due to the Schottky effect [13]. We believe that this explanation can be extended to insulator photocathodes, such as CsI, thus stating that the field enhancement of the photoemission is essentially due to surface phenomena. Let us consider a simple model, based on this hypothesis.

Fig.6 shows an energy diagram near an insulator/vacuum interface. A photoemission process consists of three stages: an electron photoexcitation from a valence to a conduction band, a transport to the surface and an escape to vacuum [7, 25, 26]. After the first stage, photoelectrons in the conduction band are distributed within the energy interval:

$$E_{pe} = \hbar\omega - E_g \tag{6}$$

(where $\hbar\omega$ is the photon energy, E_g the band gap energy), with a spectrum determined by the electron energy distribution in the valence band.

The simplification of the proposed model is that this energy spectrum is considered to be constant. It can be justified if the electron energy distribution in the valence band, in the first approximation, is flat. It is also assumed that the shape and the width of the photoelectron spectrum are not significantly disturbed during a photoelectron transport to the surface. Such strong assumption can be applied only for a restricted class of photoemmiters, like alkali halides, in which the electron have a rather large mean-free-path for inelastic collisions in the conduction band.

Our next assumption is that the electron velocity vector is isotropically distributed over a solid angle, due to a randomization caused by either elastic, electron-phonon collisions in the conduction band or other processes.

A photoelectron can escape into vacuum, if the component of its energy normal to the surface, measured from the bottom of the conduction band, exceeds the potential barrier, i.e. an electron affinity E_a (see Fig.6). Otherwise, the photoelectron will be reflected back to the bulk. Here we make another simplification: after reflection from the barrier, the photoelectron is considered to be lost. It is also supposed that each photon produces one photoelectron in the conduction band.

With the assumptions made before, a quantum efficiency is simply equal to the fraction of the photoelectron energy, higher than E_a, or more accurately, to the fraction of the normal energy component, higher than E_a, integrated over a solid angle (the derivation of the formula is presented in the Appendix):

$$QE = \frac{1}{2E_{pe}}[E_{pe} - E_a(1 + ln\frac{E_{pe}}{E_a})] \tag{7}$$

It is well known that an electric field can reduce the electron work function of metals by an amount $e(eF)^{1/2}$ due to the Schottky effect (e is the electron charge, F the electric field strength). For example, at 100 kV/cm this decrease is equal to 0.12 eV. The nature of the electron affinity of some insulators is similar to that of metals: it is due to the interaction of an electron with its electric image, induced by a medium polarization [28]. Therefore the Schottky effect can also apply to insulators [29]:

$$\Delta E_a = e(\alpha eF)^{1/2} \; ; \quad \alpha = (\epsilon_\infty - 1)/(\epsilon_\infty + 1) \tag{8}$$

Here ΔE_a is the field-induced electron affinity decrease, ϵ_∞ the high-frequency dielectric constant. For CsI: $\epsilon_\infty = 2.69$ [30] and $\alpha = 0.45$, so that that the magnitude of the Shottky effect for CsI is of the same order as that for metals.

Substituting (8) into (7) we get for the QE, in the presence of the electric field:

$$QE = \frac{1}{2E_{pe}}\{E_{pe} - [E_a - e(\alpha eF)^{1/2}][1 + ln\frac{E_{pe}}{E_a - e(\alpha eF)^{1/2}}]\} \tag{9}$$

In the case of the condition $ln(E_{pe}/E_a) \gg 1$, which is satisfied at wavelengths shorter than 185 nm, the expression may be simplified:

$$QE \approx const[1 + \frac{ln\frac{E_{pe}}{E_a}e^{3/2}\alpha^{1/2}}{E_{pe} - E_a(1 + ln\frac{E_{pe}}{E_a})}F^{1/2}] \tag{10}$$

thus following a $F^{1/2}$ law, observed in the experiment.

Only two parameters are free in the model: E_a and E_g. Since for CsI the value of $E_g + E_a = 6.3$ eV is known with good accuracy, we can fix both of them, using the expression (7) for the QE and following the experimental QE dependence of CsI on the wavelength [12]: $E_a = 0.2$ eV and $E_g = 6.1$ eV. As one can see from Fig.7, showing the QE dependence of CsI on wavelength, a good agreement is observed between the theory and the experiment with these values of E_a and E_g.

The QE dependence on the field at 160, 185 and 195 nm, predicted by the model according to expression (9), are shown in Fig.3: theoretical curves are in a reasonable agreement with the experimental data points.

In the frame of this model it is also possible to explain the field enhancement independence of the photocathode aging under electron bombardment (Fig.2). The reason could be that the energetic electron bombardment only results in a modification of the structure of the bulk, but not of the surface, the latter being responsible for the enhancement effect. The radiation-induced modification of the bulk structure, in particular an ion vacancy production, may lead to photoelectron trapping, resulting in a QE decrease, without significant modification of the photoelectron energy spectrum.

We may conclude that despite of the simplicity of the model, it is able to predict the dependence of the photoemission on the field. This allows one to use this model for an estimation of the field effect on other insulator photocathodes.

4.2 Secondary electron emission

SEE results are more difficult to explain by a simple model: besides the mentioned geometrical factors, which hinder the interpretation, the energy spectrum of secondary electrons in CsI is not so trivial as was supposed in the case of photoemission. Also, probably field-induced bulk phenomena can not be ignored due to a rather large volume occupied by an electron cascade.

However, our results can be compared with those obtained with porous alkali halide films [15, 16]. It was reported that the SEE-yield of such films has a strong dependence on the field for primary electron energies higher than 5 keV, reaching an enhancement of about 4, and is independent of the field for lower energies [15]. This is very similar to our observation (see Fig.4,5). It was shown in these works, that the SEE enhancement is caused by high electric fields, of about 10-30 kV/cm, created by an upcharging of the film surface due to a high resisivity of porous films. This is also in accordance with what we measured.

4.3 Practical applications of the field enhancement effect

Obviously, the wire-photocathode cannot be practically used, since its sensitive area is too small. Therefore, one should find ways to create high electric fields at the surface of plate-photocathodes. Yet, we see two practical solutions to create high fields in gaseous multipliers coupled to solid photocathodes.

The first is to couple photocathodes to parallel plate avalanche chambers, operating at a high gas pressure, with gases requiring high operation potentials like i-C_4H_{10}. In such case one can reach for example a field strength of the order of 60 kV/cm at 1 atm [31]. As it was shown in [12], the operation in a gas multiplication mode in a parallel-plate geometry, results in QE values compared to those of vacuum, independently of the type of the gas.

Another possible solution, being investigated by us, is to place a fine grid very close to the photocathode surface. One can thus apply a high electric field accross the thin gas gap. In principle there should be no avalanche development, and therefore no breakdown, in this narrow gap, if its size is kept below the electron inelastic mean-free-path. Methods of vacuum deposition of fine mesh structures, on top of the photocathode surface, are investigated as well.

5 Conclusions

We have measured the photocurrent and the secondary electron emission current from CsI as a function of the electric field strength in the range 1-500 kV/cm, using a multiwire cathode. The results of the present work may be summarized as follows:

- A strong field enhancement of the photoelectric emission from CsI has been observed: at 500 kV/cm the QE increase is of a factor of 1.5 at 160 nm, 3 at 185 nm and 25 at above 200 nm. At 160 nm and 185 nm this enhancement has been found to be a linear function of the square root of the field strength, being independent of the photocathode aging.

- We interpret the field enhancement of the photoemission as being essentialy a surface phenomenon, namely a field-induced decrease of the electron affinity. We presented a simple model based on this interpretation, which describes fairly well the experimental data. This model may be valid for other insulator photocathodes, operated at high electric fields.

- The magnitude of the field enhancement of the electron-induced secondary electron emission is a function of the primary electron energy: it varies from a factor of 2 at 1 keV to a factor of 10 at 5 keV. A major increment in the enhancement occurs at a moderate field, of about 10 kV/cm.

The considerable field enhanced photoemission observed in gas media [12] and in vacuum , in the present work, helps to explain some results concerning CsI operation under gas multiplication. It provides some ideas for future design of gaseous detectors combining solid electron emission convertors. In particular, the field enhancement effect can explain the QE increase observed in CsI photocathodes after gas breakdown and under high photon flux irradiation, mentioned in section 1. This suggests to search for solutions of creating high electric fields at insulator surfaces for practical applications.

Acknowledgements

We would like to thank Drs. A.Akkerman and G.Malamud for stimulating discussions.

This work was supported by the Foundation Mordoh Mijan de Salonique, by the Basic Research Foundation of the Israel Academy of Sciences and Humanities, and by the United States-Israel Binational Science Foundation (BSF). A.Buzulutskov is grateful to the Feinberg Graduate School for his support.

Appendix

Under the asumptions of our model, photoelectrons in the conduction band, near the insulator/vacuum interface, are uniformly distributed in energy and solid angle: $dN/dEd\Omega = n_0 = const$. The total number of the photoelectrons is:

$$N_{tot} = \int_0^{E_{pe}} \int_\Omega \frac{dN}{dEd\Omega} dEd\Omega = 4\pi E_{pe} n_0 \qquad (11)$$

Here Ω is the solid angle; ϕ and θ are the azimuthal and the polar angles, correspondingly.

The photoelectron can escape from the conduction band to vacuum if its maximum energy, E_{pe}, and its energy component normal to the insulator surface, $Ecos\theta$, are higher than the electron affinity E_a. The number of the photoelectrons escaping to vacuum is calculated by integrating the photoelectron distribution over the energy and the solid angle, with an account of these conditions using the Θ-functions:

$$N_{esc} = \int_0^{E_{pe}} \int_\Omega \frac{dN}{dEd\Omega} \Theta(E_{pe} - E_a)\,\Theta(Ecos\theta - E_a)\,dEd\Omega =$$
$$= 2\pi n_0 \int_0^{E_{pe}} \int_{-1}^{1} \Theta(E_{pe} - E_a)\,\Theta(Ecos\theta - E_a)\,dEd(cos\theta) =$$
$$= 2\pi n_0 [E_{pe} - E_a(1 + ln\frac{E_{pe}}{E_a}] \qquad (12)$$

In the calculation of the integral over E and $cos\theta$, we used the fact that it is equal to the hatched area, shown in Fig.8.

Since, by the assumption, each photon produces one photoelectron in the conduction band, the quantum efficiency is $QE = N_{esc}/N_{tot}$. With an account of (11) and (12) it is equal to:

$$QE = \frac{1}{2E_{pe}}[E_{pe} - E_a(1 + ln\frac{E_{pe}}{E_a})] \qquad (13)$$

References

[1] G.R.Carruthers, Appl. Opt., **14**, 1667 (1975).

[2] J.Seguinot, G.Charpak, Y.Giomataris, V.Peskov, J.Tischhauser and T.Ypsilantis, Nucl. Instr. Meth. **A297**, 133 (1990).

[3] P.Miné, Photoemissive materials and their application to gaseous detectors, Preprint X-LPNHE/93-09, Proc. of the First Workshop on RICH Detectors, Bari, Italy, June 2-5, 1993. To be published in Nucl. Instr. Meth. A, and references therein.

[4] A.Breskin, R.Chechik, D.Vartsky, G.Malamud and P.Miné, A correction of the quantum efficiency of CsI and other photocathodes due to the recalibration of the reference photomultipliers, Preprint WIS-93/116/Dec.-PH. Submitted to Nucl. Instr. Meth. A.

[5] S.A.Schwarz, J. Appl. Phys. **68**, 2382 (1990), and references therein.

[6] A.Gibrekhterman, A.Akkerman, A.Breskin and R.Chechik, J. Appl. Phys. **74**, 7506 (1993), and references therein.

[7] A.H.Sommer, Photoemissive materials, Robert E.Krager Publ. Co., Huntington, New York, 1980.

[8] V.Dangendorf, A.Breskin, R.Chechik and H.Schmidt-Böcking, Nucl. Instr. Meth. **A289**, 322 (1990).

[9] G.Charpak, V.Peskov, D.Scigocki and V.Valbis, Proc. Int. Simp. on Particle Identification at High Luminosity Hadron Colliders (ed. T.G.Gouraly and I.G.Morfin), FNAL, IL, USA, p.295 (1989).

[10] V.Dangerdorf, A.Breskin, R.Chechik and H.Schmidt-Böcking, Nucl. Instr. Meth. **A308**, 519 (1991).

[11] I.Frumkin, A.Breskin, R.Chechik, V.Elkind and A.Notea, Nucl. Instr. Meth. **A329**, 337 (1993).

[12] A.Breskin, A.Buzulutskov, R.Chechik, D.Vartsky, G.Malamud and P.Miné, Electric field effects on the quantum efficiency of CsI photocathodes in gas media, Preprint WIS-93/115/Dec.-PH. To be published in Nucl. Instr. Meth. A.

[13] J.A.Cochrane and R.F.Thumwood, Advances in Electronics and Electron Physics, **40A**, 442 (1976).

[14] J.S.Escker, Semiconductors and Materials **15**, 257 (1981), and references therein.

[15] G.W.Goetze, A.H.Boerio, M.Green, J. Appl. Phys. **35**, 482 (1964).

[16] E.L.Garwin, J.Llacer, J. Appl. Phys. **41**, 1489 (1970).

[17] G.Malamud, P.Miné, D.Vartsky, A.Breskin and R.Chechik, Nucl. Instr. Meth. **A335**, 136 (1993).

[18] A.Braem, A.DiMauro, E.Nappi, A.Ljubicic, G.Paic, F.Piuz, F.Poza, R.S.Ribeiro, T.Scognetti, T.D.Williams, Fast RICH detector with a cesium iodide photocathode at atmospheric pressure, Preprint CERN/PPE/93-209, Proc. of the First Workshop on RICH Detectors, Bari, Italy, June 2-5, 1993. To be published in Nucl. Instr. Meth. A.

[19] D.F.Anderson, S.Kwan and V.Peskov, CsI and some new photocathodes, Preprint Fermilab-Conf-93/128, Proc. of the First Workshop on RICH Detectors, Bari, Italy, June 2-5, 1993. To be published in Nucl. Instr. Meth. A.

[20] F.Sauli, Principle of operation of multiwire proportional and drift chambers, in: "Experimental Techniques in High Energy Physics" ,ed. T.Ferbel, Addison-Wesley Publ. Co., 1987.

[21] G.A.Erskine, Nucl. Instr. Meth. **105**, 565 (1972).

[22] E.Aprile, A.Bolotnikov, D.Chen, R.Mukherjee, F.Xu, D.F.Anderson, and V.Peskov, Nucl. Instr. Meth. **A338**, 328 (1994).

[23] I.M.Bronshtein, B.S.Fraiman, Secondary electron emission, Nauka, Moscow, 1969, p.245, p.283-293 (in Russian).

[24] A.Gibrekhterman, A.Akkerman, A.Breskin and R.Chechik, The spatial characteristics of electron- and photon-induced secondary electron cascades in CsI, Preprint WIS-93/120/Dec.-PH, submitted to J. Appl. Phys.

[25] W.E.Spicer, A.Herrera-Gomez, Modern theory and application of photocathodes, Preprint SLAC-PUB-6306, SLAC/SSRL-0042 (1993).

[26] A.Akkerman, T.Boutboul, A.Breskin and R.Chechik, Low energy electron transport in alkali halides. Preprint WIS-94/12/Feb.-PH, submitted to J. Appl. Phys.

[27] R.T.Poole, J.G.Jenkin, J.Liesegang and R.C.G.Leckey, Phys. Rev. **B11**, 5179 (1975).

[28] J.Cazaux, Some physical descriptions of the charging effects in insulators, in: "Ionization of solids by heavy particles", ed. R.A.Baragiola, Plenum Press, New York, 1993, p.325.

[29] L.N.Dobretsov and M.V.Gomoyunova, Emission electronics, Nauka, Moscow, 1966, p.163-164 (in Russian).

[30] W.B.Fowler, Physics of color centers, ed. W.B.Fowler, Acad. Press, New York, 1968.

[31] Yu.Galactionov, Yu.Kamyshkov, A.Malinin and V.Pojidaev, Nucl. Instr. Meth. **A317**, 116 (1992).

Figure captions

Fig.1 A schematic view of the experimental set-up.

a) The photoemission experiment: the UV-induced photocurrent from a CsI multi-wire photocathode is measured in vacuum.

b) The secondary electron emission experiment: the currrent from the CsI multi-wire SEE-cathode, induced by primary electrons photoproduced at the plate CsI photocathode, is measured in vacuum.

Fig.2 Relative quantum efficiency of CsI as a function of the electric field strength. The voltage applied to anode meshes is shown as well. Two data sets are presented: for a fresh photocathode and for an aged one (see text). Data points are normalized to the point measured with the fresh photocathode, at the lowest field value.

Fig.3 Normalized quantum efficiency of CsI as a function of the square root of the electric field strength at 160 and 185 nm (a) and at $\geq$200 nm (b). Curves are the model predictions according to the expression (9). Each data set is normalized to the point at the lowest field value.

Fig.4 Relative secondary electron emission yield from CsI, at different electric fields, as a function of the primary electron energy (symbols). Data of the absolute total SEE-yield from CsI from ref. [23] is also shown (curve).

Fig.5 Relative secondary electron emission yield from CsI for different primary electron energies, as a function of the electric field strength. The voltage applied to the anode meshes is shown as well.

Fig.6 Energy diagram at the insulator/vacuum interface. E_v is the width of the valence band; E_g the band gap energy; E_{pe} the width of the photoelectron energy spectrum in the conduction band; E_a the electron affinity.

Fig.7 The quantum efficiency of CsI, in vacuum, as a function of the wavelength. Data points are taken from ref.[12]; the curve is the model prediction according to the expression (7) with $E_g = 6.1$ eV and $E_a = 0.2$ eV.

Fig.8 Limits of the integration in formula (12).

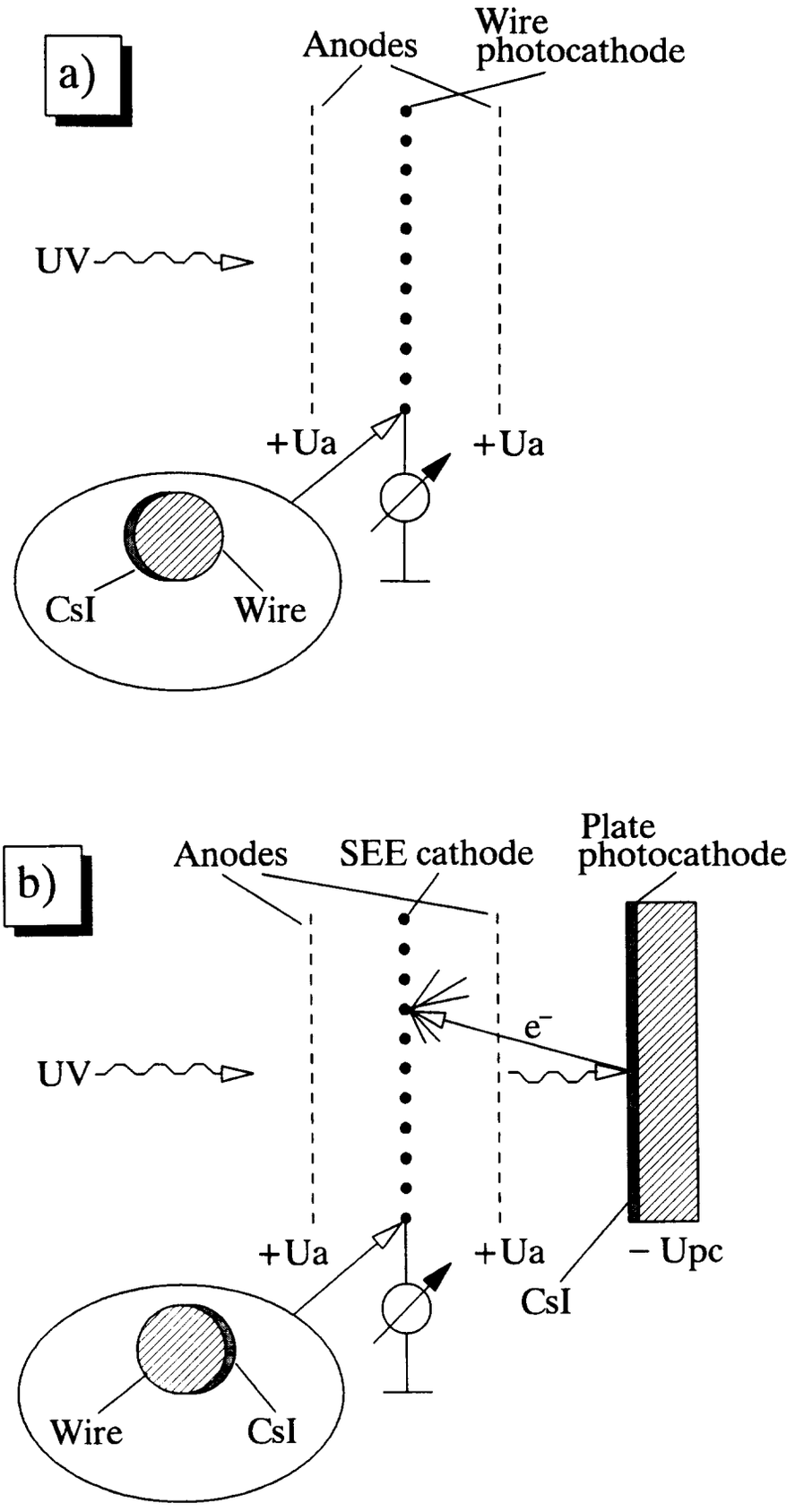
a)
Anodes
Wire photocathode
UV
+Ua
+Ua
CsI
Wire
b)
Anodes
SEE cathode
Plate photocathode
e⁻
UV
+Ua
+Ua
− Upc
CsI
Wire
CsI

Fig. 1

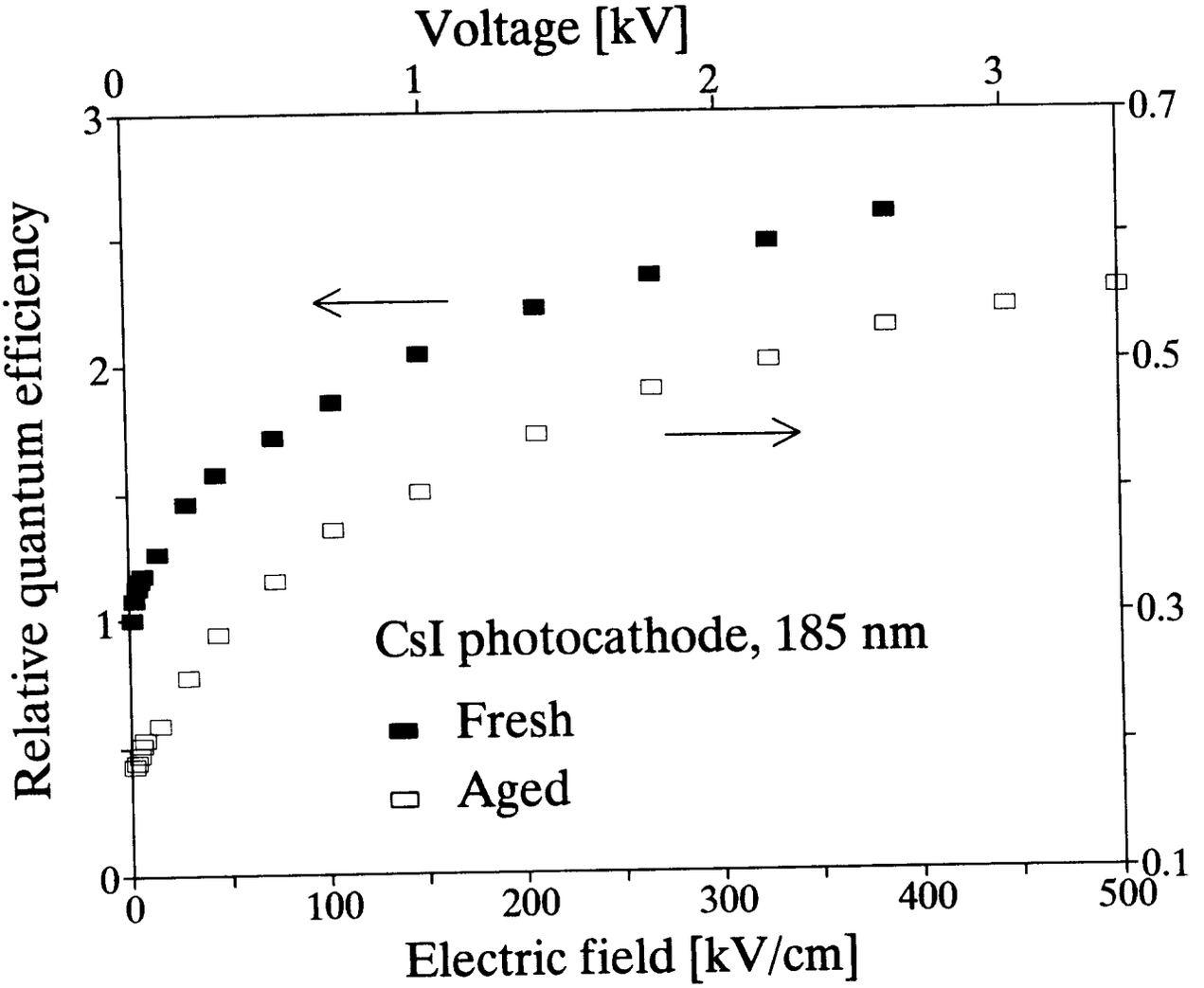
Voltage [kV]
0
1
2
3
Relative quantum efficiency
3
2
1
0
0.7
0.5
0.3
0.1
CsI photocathode, 185 nm
Fresh
Aged
0
100
200
300
400
500
Electric field [kV/cm]

Fig. 2

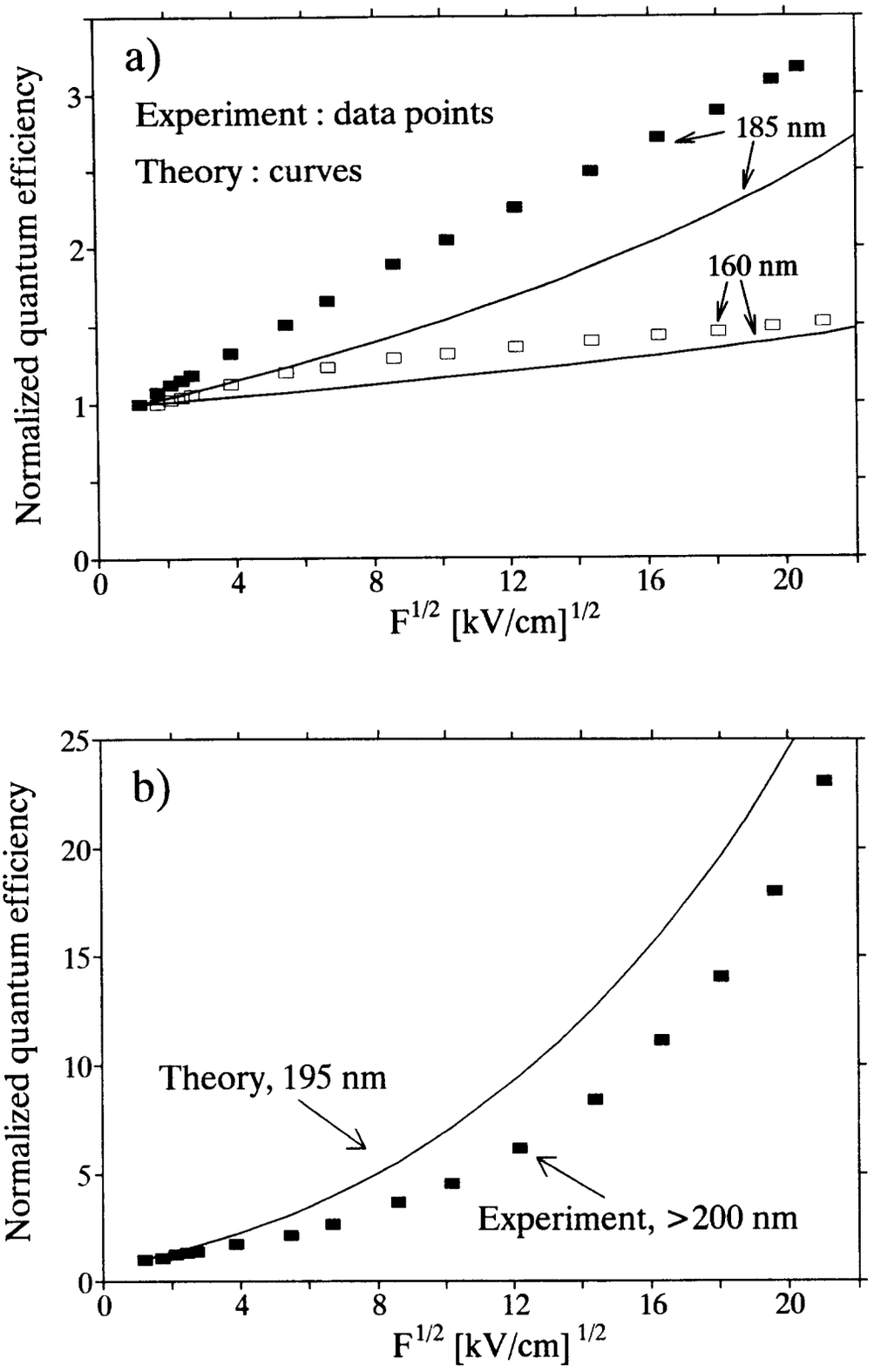
a)
Experiment : data points
Theory : curves
185 nm
160 nm
Normalized quantum efficiency
F^1/2 [kV/cm]^1/2
b)
Theory, 195 nm
Experiment, >200 nm
Normalized quantum efficiency
F^1/2 [kV/cm]^1/2

Fig. 3

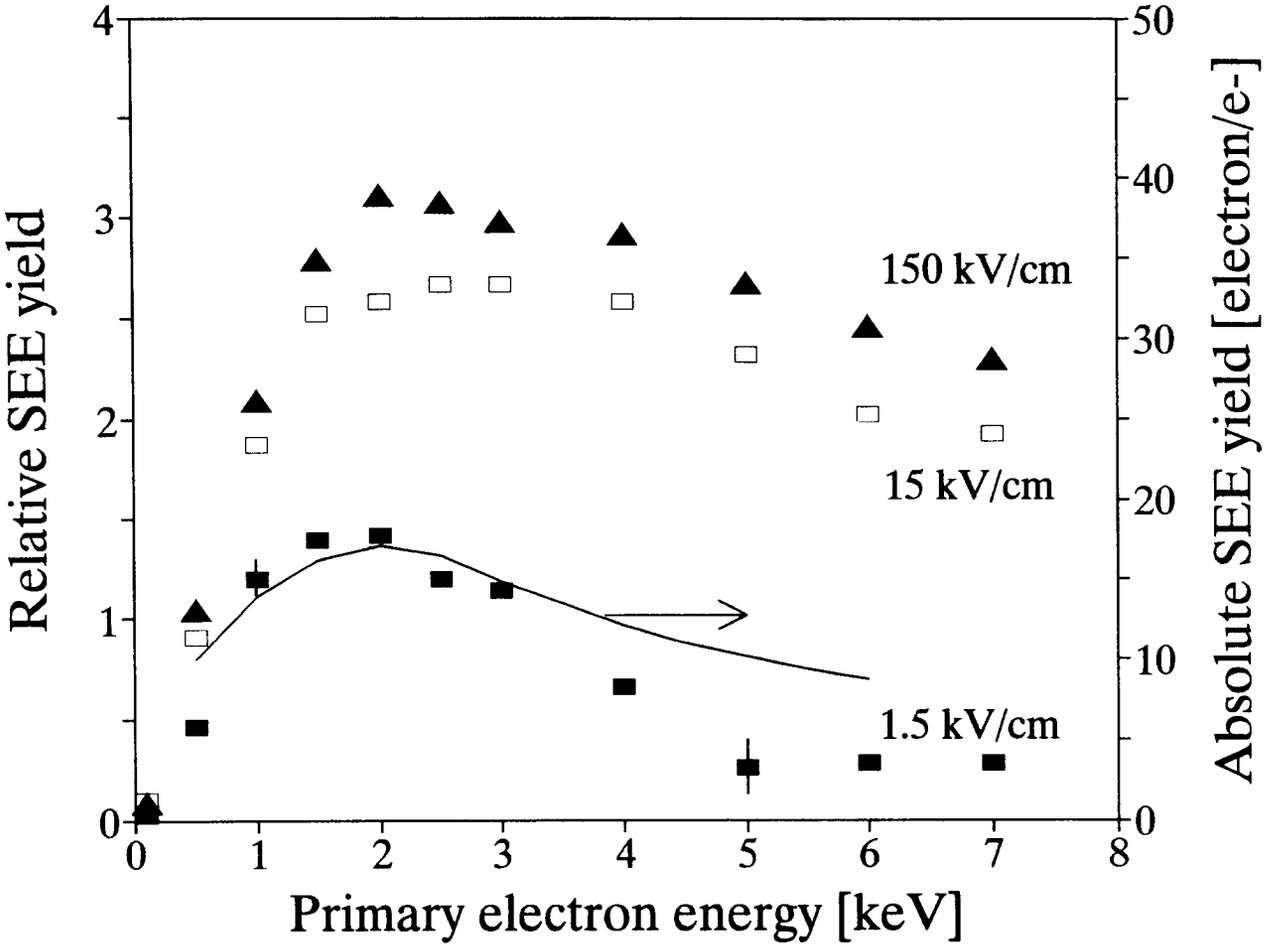
Relative SEE yield
Absolute SEE yield [electron/e-]
Primary electron energy [keV]
150 kV/cm
15 kV/cm
1.5 kV/cm
0
1
2
3
4
5
6
7
8
10
20
30
40
50

Fig. 4

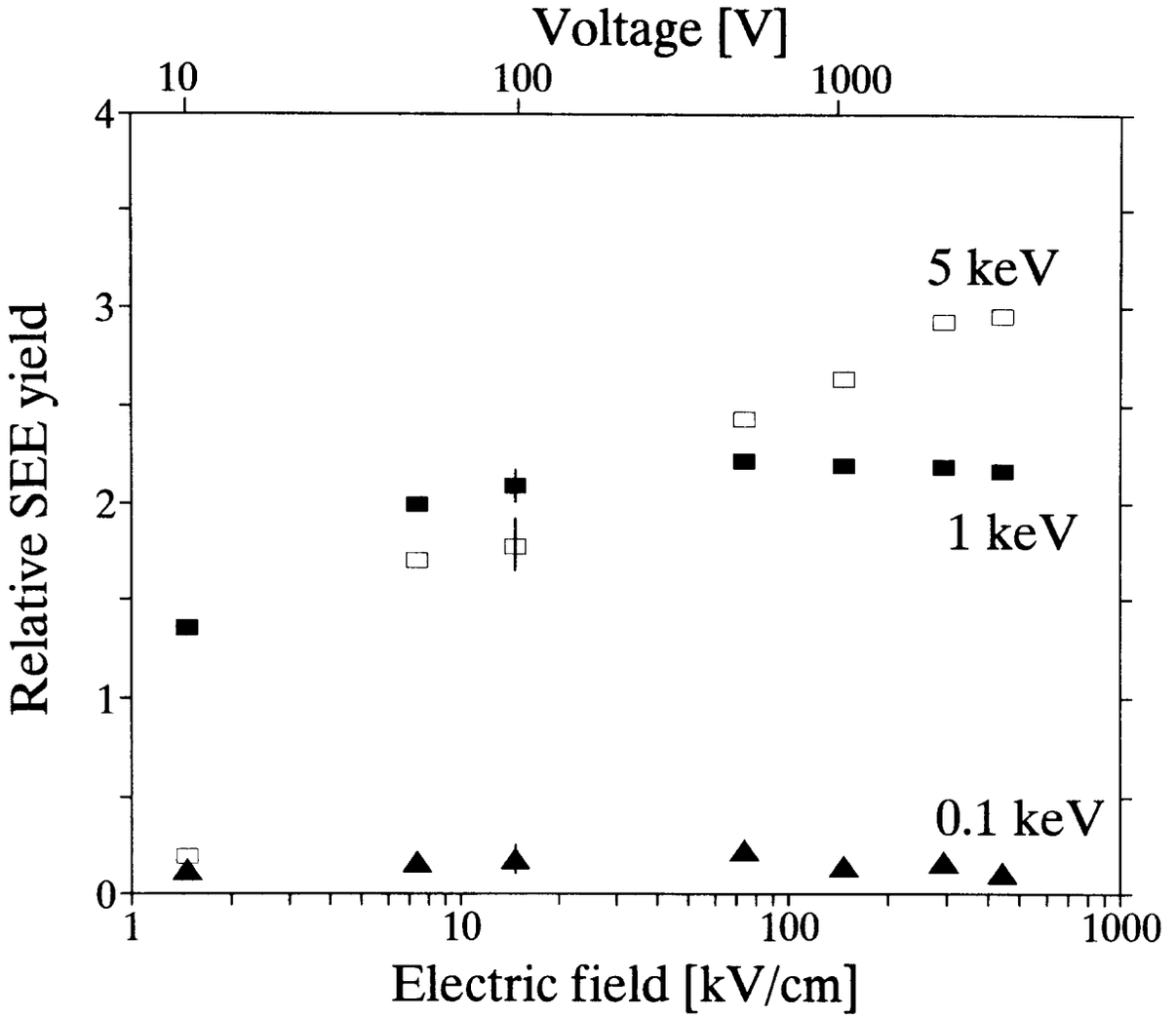
Voltage [V]
10
100
1000
4
3
2
1
0
Relative SEE yield
5 keV
1 keV
0.1 keV
1
10
100
1000
Electric field [kV/cm]

Fig. 5

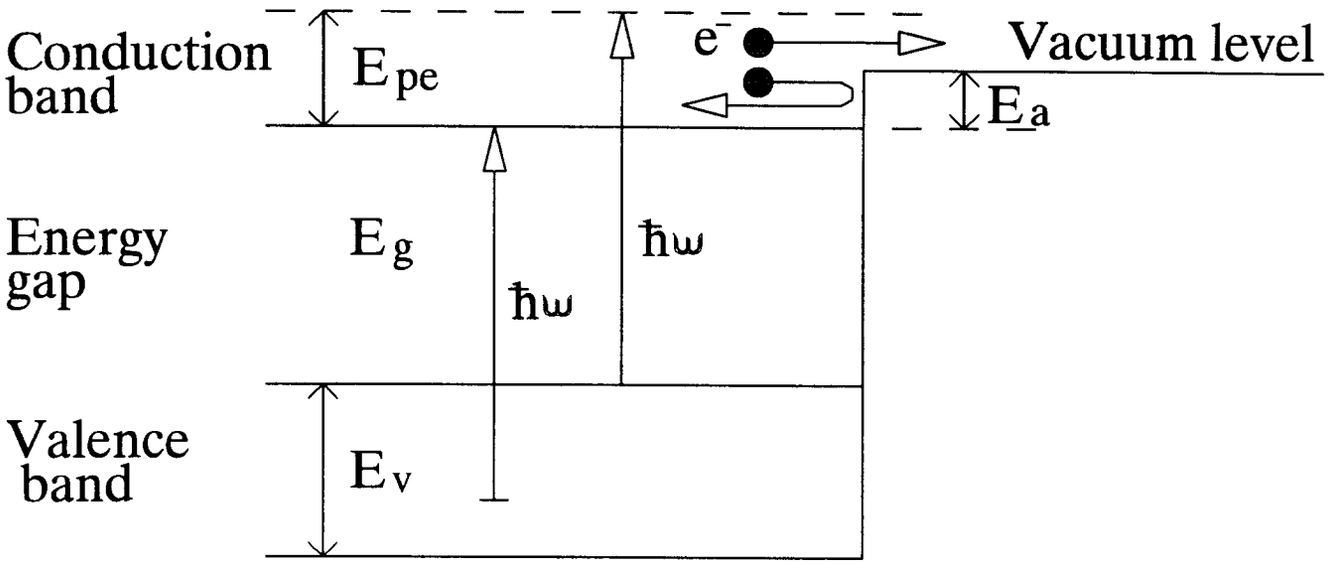
Conduction band
Energy gap
Valence band
E_{pe}
E_g
E_v
$\hbar\omega$
$\hbar\omega$
e^-
Vacuum level
E_a

Fig. 6

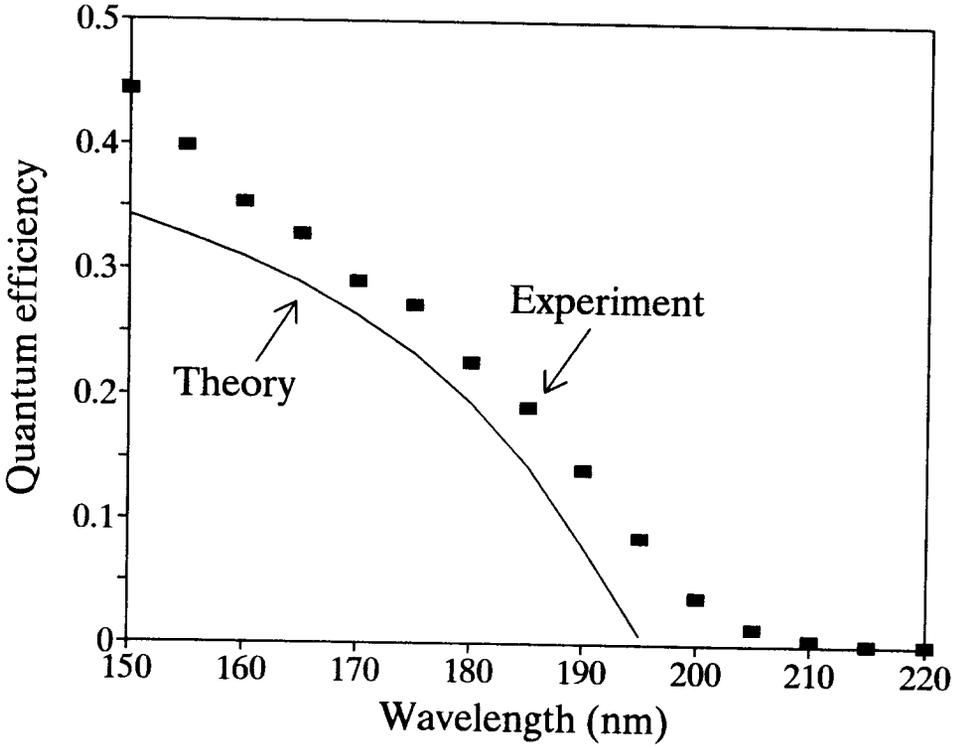
0.5
0.4
0.3
0.2
0.1
0
Quantum efficiency
Experiment
Theory
150
160
170
180
190
200
210
220
Wavelength (nm)

Fig. 7

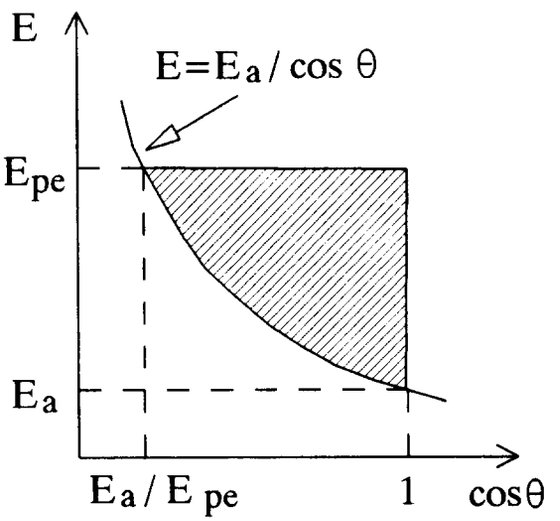
E
E=Ea / cos θ
Epe
Ea
Ea / E pe
1
cosθ

Fig. 8